Dielectric response and quantum magnetic-field effects on the screening properties of a slab of solid-state plasma

Hong-Liang Cui and Norman J. M. Horing
Department of Physics and Engineering Physics, Stevens Institute of Technology, Hoboken, New Jersey 07030

Godfrey Gumbs
Department of Physics, University of Lethbridge, Lethbridge, Alberta, Canada T1K 3M4
(Received 1 March 1990; revised manuscript received 13 September 1990)

We examine the dielectric response of a slab of quantum magnetoplasma subject to arbitrary electrostatic fields having no special symmetry across the slab. We construct the inverse dielectric function for this system in the random-phase approximation including the role of "nondiagonal" quantum interference effects, and discuss various limits and approximations of special interest. In this, we assume that the boundary conditions at the slab faces are those of specular reflection (infinite-barrier model). This work is applied to a determination of magnetic-field effects on the static shielded potential for a point charge and image phenomena in the vicinity of a slab face, including Thomas-Fermi (Debye) shielding phenomena and Friedel-Kohn "wiggle" (i.e., spatial oscillatory structure) shielding effects for a highly anisotropic magnetoplasma in the quantum strong-field limit. In this connection, shielded image potentials are examined for both source and field points outside the plasma, surface-corrected bulk shielding is treated when both points are inside the plasma, and "cross-boundary" shielding is studied when one of the points is inside the plasma boundary and the other is outside.

I. INTRODUCTION: POTENTIALS OF A SLAB OF QUANTUM MAGNETOPLASMA

As interest in semiconductor microstructures mounts, it is appropriate to reexamine the nonlocal dynamic dielectric response properties for a quantum plasma slab of *finite thickness,* bounded by two infinite-barrier-potential walls. In this study we undertake such a reexamination, employing Newns's formulation[1] for electrostatic fields which are symmetric or antisymmetric across the slab, making the useful extension to arbitrary fields having no special symmetry, and displaying the results in terms of the corresponding inverse dielectric function for the slab[2(a)]—whose general importance is tied to its close relation to the slab density-density correlation function. Our results for the slab inverse dielectric function generalize those of Bechstedt and Enderlein[2(b)] by incorporating the role of "nondiagonal" quantum interference effects. Moreover, because of its intrinsic interest, we carry out here the calculation of the statically shielded Coulomb potential of a magnetoplasma near a bounding surface using the slab inverse dielectric function, inspecting the roles of both anisotropic Thomas-Fermi-pole contributions and Friedel oscillatory contributions under high-magnetic-field conditions. This formulation is also applied in a companion paper[3] to the explicit determination of fast particle energy loss to a slab of solid-state plasma.

Our determination of the inverse dielectric function $K(1,1')=\delta V(1)/\delta U(1')$ [$U(1')$ is the impressed potential at space-time point $1'$; $V(1)$ is the effective potential at space-time point 1] for a solid-state plasma slab will employ the fact that with the model potential $U(2)=\delta^4(2-1')$, we have

$$V(1)=\int d^4 2\, K(1,2)U(2)=K(1,1')\ ,$$

which relates $K(1,1')$ directly to the corresponding effective potential $V(1)$ which we calculate by standard procedures. For the slab (Fig. 1) having infinite-barrier

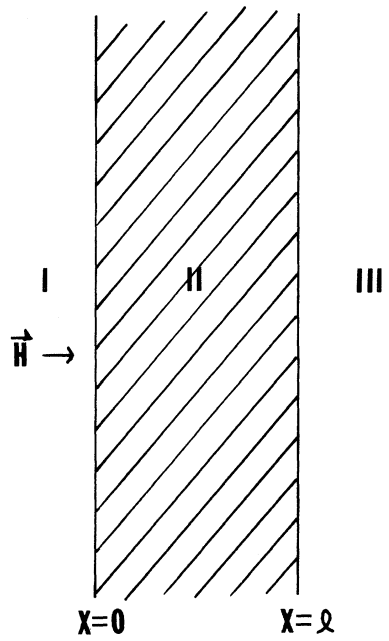

FIG. 1. Quantum plasma slab bounded by specularly reflecting hard walls at $x=0$ and $x=l$ in a normal magnetic field.

specular-reflection boundary conditions at the planar faces $x=0$ and $x=l$, we employ a mixed representation with $\bar{Q}$ as Fourier transform wave vector conjugate to $\bar{R}=\bar{r}_1-\bar{r}'_1=(y_1-y'_1, z_1-z'_1)$, and a direct x representation for which we employ a complete set of Fourier-series $\cos(qx)$ functions to represent potentials having no definite symmetry cross the slab, instead of dealing separately with symmetric and antisymmetric cases. Thus, we have

$$f(\bar{R},x)=\frac{2}{l}\sum_q \eta_q \int \frac{d^2Q}{(2\pi)^2} e^{i\bar{Q}\cdot\bar{R}}\cos(qx) f_{Qq} \ , \tag{1}$$

where

$$f_{Qq}=\int_0^l dx \int d^2R \ e^{-i\bar{Q}\cdot\bar{R}}\cos(qx) f(\bar{R},x) \tag{2}$$

with

$$q=\frac{n\pi}{l}, \quad n=0,1,2,\ldots, \tag{3a}$$

and

$$\eta_q=\begin{cases}\frac{1}{2} & \text{for } q=0\\ 1 & \text{for } q>0 \ .\end{cases} \tag{3b}$$

Following Newns's notation,[1] we consider arbitrary external sources $S^{\rm I}, S^{\rm II}, S^{\rm III}$ localized in regions I, II, III, which produce potential contributions $U^{\rm I}, U^{\rm II}, U^{\rm III}$, respectively ($\nabla^2 U=4\pi S$). Furthermore, we designate the perturbed slab density as $\delta\rho(1)$, and the associated density perturbation response function as $R(1,2)=\delta\rho(1)/\delta V(2)\rightarrow\delta\rho(1)=\int d^4 2\, R(1,2)V(2)$, which has a double-Fourier-series representation $R(x,x')\rightarrow R_{qq'}\rightarrow R_{Qqq'}$. In these terms, the Poisson equation for the slab yields

$$V_Q(x)=-\frac{2}{l}\sum_q \eta_q\cos(qx) \times\sum_{q'} E^{-1}{}_{Qqq'}[4\pi S^{\rm II}_{Qq'}+V'_Q(0) -(-1)^{n'}V'_Q(l)] \ , \tag{4}$$

where $V'_Q(0), V'_Q(l)$ represent derivatives of V at the boundaries $x=0$ and $x=l$ and ($|\mathbf{q}|^2=Q^2+q^2$)

$$E_{Qqq'}=|\mathbf{q}|^2\delta_{qq'}/\eta_q+4\pi R_{Qqq'} \tag{5a}$$

and the structure of $R_{Qqq'}$ is

$$R_{Qqq'}=D_{Qq}\delta_{qq'}/\eta_q-A_{Qqq'} \ , \tag{5b}$$

with a "diagonal" part, D_{Qq}, and a "nondiagonal" part, $-A_{Qqq'}$. Consideration of the electrostatics of the regions I and III outside the slab yields

$$V'_Q(0)=QV_Q(0)-2QU^{\rm I}_Q(0) \ , \tag{6a}$$

$$V'_Q(l)=-QV_Q(l)+2QU^{\rm III}_Q(l) \ , \tag{6b}$$

which may be used in conjunction with Eq. (4) to determine $V_Q(0)$ and $V_Q(l)$ as

$$V_Q(0)=\frac{(1-\tilde{A})S_1+BS_2}{(1-A)(1-\tilde{A})-B^2} \ , \tag{7a}$$

$$V_Q(l)=\frac{(1-A)S_2+BS_1}{(1-A)(1-\tilde{A})-B^2} \ . \tag{7b}$$

In the evaluation of $S_1, S_2, A, \tilde{A}, B$, we employ the fact that $E^{-1}{}_{Qqq'}$ is the (q,q') matrix element of the operator $E^{-1}{}_Q$, such that $E^{-1}{}_{Qqq'}=\langle q|(E^{-1}{}_Q)|q'\rangle$, which is the inverse of the dielectric matrix of Eq. (5a), involving only the density perturbation response function R_Q. Recognizing that R_Q has even parity about the center of the slab, it follows that E_Q and $E^{-1}{}_Q$ also have even parity, so that the states $\langle q|$ and $|q'\rangle$ must have the same parity to have a nonvanishing matrix element $E^{-1}{}_{Qqq'}$. With this in view, we find that

$$A=\tilde{A}=-1/2\epsilon_Q-1/2\tilde{\epsilon}_Q, \quad B=1/2\epsilon_Q-1/2\tilde{\epsilon}_Q \tag{8}$$

where

$$\epsilon_Q=\left[(4Q/l)\sum_{\substack{qq'\\ \text{odd}}} E^{-1}{}_{Qqq'}\right]^{-1} ,$$
$$\tilde{\epsilon}_Q=\left[(4Q/l)\sum_{\substack{qq'\\ \text{even}}} \eta_q E^{-1}{}_{Qqq'}\right]^{-1} \tag{9}$$

and

$$S_1=-\frac{8\pi}{l}\left[\sum_{q,q'\ \text{odd}}+\sum_{q,q'\ \text{even}} n_q\right]E^{-1}{}_{Qqq'}S^{\rm II}_{Qq'} +\frac{1}{\epsilon_Q(\Omega)}[U^{\rm I}_Q(0)-U^{\rm III}_Q(l)] +\frac{1}{\tilde{\epsilon}_Q(\Omega)}[U^{\rm I}_Q(0)+U^{\rm III}_Q(l)] \tag{10}$$

and

$$S_2=-\frac{8\pi}{l}\left[-\sum_{q,q'\ \text{odd}}+\sum_{q,q'\ \text{even}} \eta_q\right]E^{-1}{}_{Qqq'}S^{\rm II}_{Qq'} -\frac{1}{\epsilon_Q(\Omega)}[U^{\rm I}_Q(0)-U^{\rm III}_Q(l)] +\frac{1}{\tilde{\epsilon}_Q(\Omega)}[U^{\rm I}_Q(0)+U^{\rm III}_Q(l)] \ . \tag{11}$$

The final results for $V_Q(0)$ and $V_Q(l)$ are

$$V_Q(0)=(1+\epsilon_Q)^{-1}(1+\tilde{\epsilon}_Q)^{-1}\left[-\epsilon_Q(1+\tilde{\epsilon}_Q)\frac{8\pi}{l}\sum_{q,q'\ \mathrm{odd}}E^{-1}{}_{Qqq'}S^{\mathrm{II}}_{Qq'}-\tilde{\epsilon}_Q(1+\epsilon_Q)\frac{8\pi}{l}\sum_{q,q'\ \mathrm{even}}\eta_q E^{-1}{}_{Qqq'}S^{\mathrm{II}}_{Qq'}\right.$$
$$\left.+(2+\epsilon_Q+\tilde{\epsilon}_Q)U^{\mathrm{I}}_Q(0)+(\epsilon_Q-\tilde{\epsilon}_Q)U^{\mathrm{III}}_Q(l)\right], \tag{12}$$

$$V_Q(l)=(1+\epsilon_Q)^{-1}(1+\tilde{\epsilon}_Q)^{-1}\left[\epsilon_Q(1+\tilde{\epsilon}_Q)\frac{8\pi}{l}\sum_{q,q'\ \mathrm{odd}}E^{-1}{}_{Qqq'}S^{\mathrm{II}}_{Qq'}-\tilde{\epsilon}_Q(1+\epsilon_Q)\frac{8\pi}{l}\sum_{q,q'\ \mathrm{even}}\eta_q E^{-1}{}_{Qqq'}S^{\mathrm{II}}_{Qq'}\right.$$
$$\left.+(\epsilon_Q-\tilde{\epsilon}_Q)U^{\mathrm{I}}_Q(0)+(2+\epsilon_Q+\tilde{\epsilon}_Q)U^{\mathrm{III}}_Q(l)\right] \tag{13}$$

and using Eq. (6) we obtain $V'_Q(0)$ and $V'_Q(l)$ which facilitate an explicit determination of the potential $V_Q(x)$ as (set $\tilde{E}^{-1}{}_{Qqq'}=\eta_q E^{-1}{}_{Qqq'}$)

$$V_Q(x)=U^{\mathrm{I}}_Q(x)-e^{Qx}U^{\mathrm{I}}_Q(0)+\frac{e^{Qx}}{(1+\epsilon_Q)(1+\tilde{\epsilon}_Q)}\left[-\epsilon_Q(1+\tilde{\epsilon}_Q)\frac{8\pi}{l}\sum_{qq'\ \mathrm{odd}}E^{-1}{}_{Qqq'}S^{\mathrm{II}}_{Qq'}-\tilde{\epsilon}_Q(1+\epsilon_Q)\frac{8\pi}{l}\sum_{q,q'\ \mathrm{even}}\tilde{E}^{-1}{}_{Qqq'}S^{\mathrm{II}}_{Qq'}\right.$$
$$\left.+(2+\epsilon_Q+\tilde{\epsilon}_Q)U^{\mathrm{I}}_Q(0)+(\epsilon_Q-\tilde{\epsilon}_Q)U^{\mathrm{III}}_Q(l)\right], \tag{14}$$

for region I, $x<0$,

$$V_Q(x)=-\frac{4}{l}\sum_{q,q'\ \mathrm{odd}}\cos(qx)E^{-1}{}_{Qqq'}\left[2\pi S^{\mathrm{II}}_{Qq'}-\frac{Q\epsilon_Q}{1+\epsilon_Q}\left[\frac{8\pi}{l}\sum_{k,k'\ \mathrm{odd}}E^{-1}{}_{Qkk'}S^{\mathrm{II}}_{Qk'}+U^{\mathrm{I}}_Q(0)-U^{\mathrm{III}}_Q(l)\right]\right]$$
$$-\frac{4}{l}\sum_{q,q'\ \mathrm{even}}\cos(qx)\tilde{E}^{-1}{}_{Qqq'}\left[2\pi S^{\mathrm{II}}_{Qq'}-\frac{Q\tilde{\epsilon}_Q}{1+\tilde{\epsilon}_Q}\left[\frac{8\pi}{l}\sum_{k,k'\ \mathrm{even}}\tilde{E}^{-1}{}_{Qkk'}S^{\mathrm{II}}_{Qk'}+U^{\mathrm{I}}_Q(0)+U^{\mathrm{III}}_Q(l)\right]\right], \tag{15}$$

for region II, $0\le x\le l$,

$$V_Q(x)=U^{\mathrm{III}}_Q(x)-e^{-Q(x-l)}U^{\mathrm{III}}_Q(l)$$
$$+\frac{e^{-Q(x-l)}}{(1+\epsilon_Q)(1+\tilde{\epsilon}_Q)}\left[\epsilon_Q(1+\tilde{\epsilon}_Q)\frac{8\pi}{l}\sum_{q,q'\ \mathrm{odd}}E^{-1}{}_{Qqq'}S^{\mathrm{II}}_{Qq'}-\tilde{\epsilon}_Q(1+\epsilon_Q)\frac{8\pi}{l}\sum_{q,q'\ \mathrm{even}}\tilde{E}^{-1}{}_{Qqq'}S^{\mathrm{II}}_{Qq'}\right.$$
$$\left.+(\epsilon_Q-\tilde{\epsilon}_Q)U^{\mathrm{I}}_Q(0)+(2+\epsilon_Q+\tilde{\epsilon}_Q)U^{\mathrm{III}}_Q(l)\right], \tag{16}$$

for region III, $x>l$.

II. INVERSE DIELECTRIC FUNCTION OF A PLASMA SLAB

The most useful characterization of electrostatic response of the slab plasma is provided by the inverse dielectric function $K(1,1')$, which is a property of the medium, independent of field within the framework of linear response. It embodies a description of dynamic and nonlocal screening phenomena, including nonlocal image potentials involved in surface interactions and collective modes of the bounded slab plasma. $K(1,1')$ plays a central role in the determination of the Raman light scattering cross section, van der Waals interactions, correlation phenomena, and energy loss which we will discuss at length in the companion paper.[3] As indicated above, we will determine $K(1,1')$ using a model potential $U(2)=\delta^4(2-1')$ such that

$$V_{1'}(1)=\int d^4 2\,K(1,2)U(2)=K(1,1')\ . \tag{17}$$

It is straightforward to determine the sources of U as $\nabla^2 U=4\pi S$ and construct $K_Q(x,x',\Omega)$ using Eqs. (14)–(17), with the result

$$
\begin{aligned}
K_Q(x,x',\Omega)=\theta(-x)\Bigg[&\delta(x-x')-e^{Qx}\delta(x')+\frac{e^{Qx}}{2(1+\epsilon_Q)(1+\tilde{\epsilon}_Q)}[(2+\epsilon_Q+\tilde{\epsilon}_Q)\delta(x')+(\epsilon_Q-\tilde{\epsilon}_Q)\delta(l-x)]\\
&+\theta(x')\theta(l-x')e^{Qx}\Bigg[\frac{\epsilon_Q}{1+\epsilon_Q}\frac{2}{l}\sum_{q,q'\ \mathrm{odd}}E^{-1}{}_{Qqq'}|\mathbf{q}'|^2\cos(q'x')\\
&\qquad+\frac{\tilde{\epsilon}_Q}{1+\tilde{\epsilon}_Q}\frac{2}{l}\sum_{q,q'\ \mathrm{even}}\tilde{E}^{-1}{}_{Qqq'}|\mathbf{q}'|^2\cos(q'x')\Bigg]\Bigg]\\
+\theta(x)\theta(l-x)\Bigg[&-[\delta(l-x')-\delta(x')]\frac{\epsilon_Q}{1+\epsilon_Q}\frac{2Q}{l}\sum_{q,q'\ \mathrm{odd}}\cos(qx)E^{-1}{}_{Qqq'}\\
&+[\delta(l-x')+\delta(x')]\frac{\tilde{\epsilon}_Q}{1+\tilde{\epsilon}_Q}\frac{2Q}{l}\sum_{q,q'\ \mathrm{even}}\cos(qx)\tilde{E}^{-1}{}_{Qqq'}\\
&+\theta(x')\theta(l-x')\Bigg[\frac{2}{l}\sum_{q,q'\ \mathrm{odd}}|\mathbf{q}'|^2E^{-1}{}_{Qqq'}\cos(qx)\cos(q'x')\\
&\qquad+\frac{2}{l}\sum_{q,q'\ \mathrm{even}}|\mathbf{q}'|^2\tilde{E}^{-1}{}_{Qqq'}\cos(qx)\cos(q'x')\\
&\qquad-\frac{\epsilon_Q}{1+\epsilon_Q}\frac{8Q}{l^2}\sum_{q,q'\ \mathrm{odd}}\sum_{k,k'\ \mathrm{odd}}E^{-1}{}_{Qqq'}E^{-1}{}_{Qkk'}|\mathbf{k}'|^2\cos(qx)\cos(k'x')\\
&\qquad-\frac{\tilde{\epsilon}_Q}{1+\tilde{\epsilon}_Q}\frac{8Q}{l^2}\sum_{q,q'\ \mathrm{even}}\sum_{k,k'\ \mathrm{even}}\tilde{E}^{-1}{}_{Qqq'}\tilde{E}^{-1}{}_{Qkk'}|\mathbf{k}'|^2\cos(qx)\cos(k'x')\Bigg]\Bigg]\\
+\theta(x-l)\Bigg[&\delta(x-x')-e^{-Q(x-l)}\delta(l-x')+\frac{e^{-Q(x-l)}}{2(1+\epsilon_Q)(1+\tilde{\epsilon}_Q)}[(\epsilon_Q-\tilde{\epsilon}_Q)\delta(x')+(2+\epsilon_Q+\tilde{\epsilon}_Q)\delta(l-x')]\\
&-\theta(x')\theta(l-x')e^{-Q(x-l)}\Bigg[\frac{\epsilon_Q}{1+\epsilon_Q}\frac{2}{l}\sum_{q,q'\ \mathrm{odd}}E^{-1}{}_{Qqq'}|\mathbf{q}'|^2\cos(q'x')\\
&\qquad-\frac{\tilde{\epsilon}_Q}{1+\tilde{\epsilon}_Q}\frac{2}{l}\sum_{q,q'\ \mathrm{even}}\tilde{E}^{-1}{}_{Qqq'}|\mathbf{q}'|^2\cos(q'x')\Bigg]\Bigg].
\end{aligned}
\tag{18}
$$

These results, as well as Eqs. (19)–(21) below incorporate the role of "nondiagonal" quantum interference effects due to the specular reflection of electrons at the "hard wall" surfaces at $x=0$ and $x=l$, including spatial inhomogeneities induced into the structure of the polarizability by the boundary conditions.

In the semi-infinite limit, $l\to\infty$, we find[2]

$$
\begin{aligned}
K_Q(x,x',\Omega)=\theta(-x)\Bigg[&\delta(x-x')-\frac{\epsilon_Q}{1+\epsilon_Q}e^{Qx}\delta(x')+\theta(x')e^{Qx}\frac{\epsilon_Q}{1+\epsilon_Q}\frac{l}{\pi^2}\int_0^\infty dq\int_0^\infty dq'\,E^{-1}{}_{Qqq'}|\mathbf{q}'|^2\cos(q'x')\Bigg]\\
+\theta(x)\Bigg[&\delta(x')\frac{\epsilon_Q}{1+\epsilon_Q}\frac{Ql}{\pi^2}\int_0^\infty dq\int_0^\infty dq'\,E^{-1}{}_{Qqq'}\cos(qx)\\
&+\theta(x')\frac{l}{\pi^2}\int_0^\infty dq\int_0^\infty dq'\,E^{-1}{}_{Qqq'}|\mathbf{q}'|^2\cos(qx)\cos(q'x')\\
&-\theta(x')\frac{\epsilon_Q}{1+\epsilon_Q}\frac{Ql^2}{\pi^4}\int_0^\infty dq\int_0^\infty dq'\,E^{-1}{}_{Qqq'}\cos(qx)\int_0^\infty dk\int_0^\infty dk'\,E^{-1}_{Qkk'}|\mathbf{k}'|^2\cos(k'x')\Bigg].
\end{aligned}
\tag{19}
$$

Although smaller, neglected terms in $K_Q(x,x'\Omega)$ of order $O(l^{-1})$ are of importance in problems of surface physics, and denoting the associated contribution as K_Q^{surface} we obtain

$$K_Q^{\text{surface}}(x,x',\Omega)=-\theta(-x)\delta(x')e^{Qx}\frac{\alpha\epsilon_Q^2}{2(1+\epsilon_Q)^2}$$

$$+\theta(-x)\theta(x')e^{Qx}\left[-\frac{\epsilon_Q}{1+\epsilon_Q}\frac{\alpha Q}{2}+\frac{\epsilon_Q^2\alpha}{(1+\epsilon_Q)^2}\frac{l}{2\pi^2}\int_0^\infty dk\int_0^\infty dk'\,E^{-1}{}_{Qkk'}|\mathbf{k}'|^2\cos(k'x')\right]$$

$$+\theta(x)\delta(x')\left[-\frac{\epsilon_Q}{1+\epsilon_Q}\frac{\alpha}{2}+\frac{\epsilon_Q^2}{(1+\epsilon_Q)^2}\frac{\alpha l}{2\pi^2}\int_0^\infty dk\int_0^\infty dk'\cos(kx)E^{-1}{}_{Qkk'}\right]-\theta(x)\theta(x')\frac{Q\alpha}{2}$$

$$+\theta(x)\theta(x')\left[\frac{\epsilon_Q}{1+\epsilon_Q}\frac{\alpha l}{2\pi^2}\int_0^\infty dk\int_0^\infty dk'E^{-1}{}_{Qkk'}|\mathbf{k}'|^2\cos(k'x')\right.$$

$$-\frac{\epsilon_Q^2}{(1+\epsilon_Q)^2}\frac{Q\alpha l}{\pi^2}\int_0^\infty dq\int_0^\infty dq'\cos(qx)E^{-1}{}_{Qqq'}\frac{l}{2\pi^2}$$

$$\times\int_0^\infty dk\int_0^\infty dk'\,E^{-1}{}_{Qkk'}|\mathbf{k}'|^2\cos(k'x')$$

$$\left.+\frac{\epsilon_Q}{(1+\epsilon_Q)}\frac{\alpha Q^2 l}{2\pi^2}\int_0^\infty dq\int_0^\infty dq'\cos(qx)E^{-1}{}_{Qqq'}\right], \tag{20}$$

where

$$\alpha=(Q/\pi)\int_0^\infty dq'\,E^{-1}{}_{Q0q'}\,. \tag{21}$$

In the case of a thick but finite slab of solid-state plasma ($Q_F l\gg 1$), it is often useful to employ the "diagonal" approximation[1] which neglects quantum interference effects associated with the vanishing of wave functions and density at the infinite-barrier slab boundaries, while admitting to consideration bulk quantum effects arising in the temperature-dependent Lindhard dielectric function and its Landau quantized counterpart in high magnetic field. In this, only surface-induced spatially-inhomogeneous modifications of the polarizability are ignored in the process of joining bulk dielectric response properties across the boundaries of adjoining media at the slab faces (including their complement of bulk quantum effects). Such a "diagonal" approximation is also in fact exact in the semiclassical limit where the electron dynamics are governed by purely classical laws, while statistical averaging is carried out with a Fermi-Dirac distribution. In general, the "diagonal" approximation may be expected to be valid for samples which are large in comparison with the characteristic distance to which surface-induced spatial inhomogeneities penetrate the polarization properties, $l\gg(2Q_F)^{-1}$. In this case, the "nondiagonal" term $-A_{Qqq'}$ of $R_{Qqq'}$ in Eq. (5b) may be neglected, and the resulting diagonality of $R_{Qqq'}$ and $E_{Qqq'}$ yields

$$E^{-1}{}_{Qqq'}=\delta_{qq'}/[(q^2+Q^2)\epsilon(\mathbf{q},\Omega)]\,, \tag{22}$$

where

$$\epsilon(\mathbf{q},\Omega)=1+4\pi D_{Qq}/(q^2+Q^2) \tag{23}$$

is approximately the bulk quantum-mechanical dielectric function [Lindhard, generalized for temperature and magnetic field, within the random-phase approximation (RPA)] for $2Q_F l\gg 1$. Thus, in the "diagonal" approximation, $K_Q(x,x'\Omega)$ is given by the finite slab result

$$K_Q(x,x',\Omega)=\theta(-x)\left[\delta(x-x')-e^{Qx}\delta(x')+\frac{e^{Qx}}{2(1+\epsilon_Q)(1+\tilde{\epsilon}_Q)}[(2+\epsilon_Q+\tilde{\epsilon}_Q)\delta(x')+(\epsilon_Q-\tilde{\epsilon}_Q)\delta(l-x')]\right.$$

$$\left.+\theta(x')\theta(l-x')e^{Qx}\left[\frac{\tilde{\epsilon}_Q}{1+\tilde{\epsilon}_Q}\tilde{\epsilon}^{-1}(Q,x',\Omega)+\frac{\epsilon_Q}{1+\epsilon_Q}\epsilon^{-1}(Q,x',\Omega)\right]\right]$$

$$+\theta(x)\theta(l-x)\left[-[\delta(l-x')-\delta(x')]\frac{\epsilon_Q}{1+\epsilon_Q}a(Q,x,\Omega)+[\delta(l-x')+\delta(x')]\frac{\tilde{\epsilon}_Q}{1+\tilde{\epsilon}_Q}\tilde{a}(Q,x,\Omega)\right.$$

$$+\tfrac{1}{2}\theta(x')\theta(l-x')\left\{\epsilon^{-1}(Q,x+x',\Omega)+\epsilon^{-1}(Q,x-x',\Omega)+\tilde{\epsilon}^{-1}(Q,x+x',\Omega)\right.$$

$$+\tilde{\epsilon}^{-1}(Q,x-x',\Omega)-\frac{2\epsilon_Q}{1+\epsilon_Q}\epsilon^{-1}(Q,x',\Omega)a(Q,x,\Omega)$$

$$\left.\left.-\frac{2\tilde{\epsilon}_Q}{1+\tilde{\epsilon}_Q}\tilde{\epsilon}^{-1}(Q,x',\Omega)\tilde{a}(Q,x,\Omega)\right\}\right]$$

$$+\theta(x-l)\left[\delta(x-x')-e^{-Q(x-l)}\delta(l-x')\right.$$

$$+\frac{\epsilon^{-Q\{x-l\}}}{2(1+\epsilon_Q)(1+\tilde{\epsilon}_Q)}[(\epsilon_Q-\tilde{\epsilon}_Q)\delta(x')+(2+\epsilon_Q+\tilde{\epsilon}_Q)\delta(l-x')-\theta(x')\theta(l-x')\epsilon^{-Q(x-l)}]$$

$$\left.\times\left[\frac{\epsilon_Q}{1+\epsilon_Q}\epsilon^{-1}(Q,x',\Omega)-\frac{\tilde{\epsilon}_Q}{1+\tilde{\epsilon}_Q}\tilde{\epsilon}^{-1}(Q,x',\Omega)\right]\right], \tag{24}$$

where

$$\epsilon_Q(\Omega)=\left[\frac{4Q}{l}\sum_{q,q'\ \text{odd}}E^{-1}{}_{Qqq'}(\Omega)\right]^{-1}\rightarrow\left[\frac{4Q}{l}\sum_{q\ \text{odd}}\frac{1}{|\mathbf{q}|^2\epsilon(\mathbf{q},\Omega)}\right]^{-1} \tag{25a}$$

and

$$\tilde{\epsilon}_Q(\Omega)=\left[\frac{4Q}{l}\sum_{q,q'\ \text{even}}\tilde{E}^{-1}{}_{Qqq'}(\Omega)\right]^{-1}\rightarrow\left[\frac{4Q}{l}\sum_{q\ \text{even}}\frac{\eta_q}{|\mathbf{q}|^2\epsilon(\mathbf{q},\Omega)}\right]^{-1} \tag{25b}$$

and

$$\epsilon^{-1}(Q,x,\Omega)=\frac{2}{l}\sum_{q\ \text{odd}}\frac{\cos(qx)}{\epsilon(\mathbf{q},\Omega)}\ , \tag{26a}$$

$$\tilde{\epsilon}^{-1}(Q,x,\Omega)=\frac{2}{l}\sum_{q\ \text{even}}\frac{\eta_q\cos(qx)}{\epsilon(\mathbf{q},\Omega)}\ , \tag{26b}$$

$$a(Q,x,\Omega)=\frac{2Q}{l}\sum_{q\ \text{odd}}\frac{\cos(qx)}{|\mathbf{q}|^2\epsilon(\mathbf{q},\Omega)}\ , \tag{27a}$$

$$\tilde{a}(Q,x,\Omega)=\frac{2Q}{l}\sum_{q\ \text{even}}\frac{\eta_q\cos(qx)}{|\mathbf{q}|^2\epsilon(\mathbf{q},\Omega)}\ . \tag{27b}$$

These results for the "diagonal" approximation are in agreement with those of Bechstedt and Enderlein[2(b)] for slab dielectric response.

Finally, in the semi-infinite limit of the "diagonal" approximation,[2]

$$K_Q(x,x',\Omega)=\theta(-x)\left[\delta(x-x')-\frac{\epsilon_Q}{1+\epsilon_Q}e^{Qx}\delta(x')+\theta(x')e^{Qx}\frac{2\epsilon_Q}{1+\epsilon_Q}\epsilon^{-1}(Q,x',\Omega)\right]$$
$$+\theta(x)\left[\delta(x')\frac{\epsilon_Q}{1+\epsilon_Q}a(Q,x,\Omega)+\theta(x')[\epsilon^{-1}(Q,x-x',\Omega)+\epsilon^{-1}(Q,x+x',\Omega)]\right.$$
$$\left.-\theta(x')\frac{2\epsilon_Q}{1+\epsilon_Q}a(Q,x,\Omega)\epsilon^{-1}(Q,x',\Omega)\right], \tag{28}$$

where

$$\epsilon_Q^{-1}(\Omega)=\frac{Ql}{\pi^2}\int_0^\infty dq\int_0^\infty dq'\frac{2\pi}{l}\frac{\delta(q-q')}{|\mathbf{q}'|^2\epsilon(\mathbf{q},\Omega)}$$
$$=\frac{2Q}{\pi}\int_0^\infty dq\frac{1}{|\mathbf{q}|^2\epsilon(\mathbf{q},\Omega)} \tag{29}$$

and

$$\epsilon^{-1}(Q,x,\Omega)=\frac{1}{\pi}\int_0^\infty dq\frac{\cos(qx)}{\epsilon(\mathbf{q},\Omega)} \tag{30}$$

and

$$a(Q,x,\Omega)=\frac{2Q}{\pi}\int_0^\infty dq\frac{\cos(qx)}{|\mathbf{q}|^2\epsilon(\mathbf{q},\Omega)}\ . \tag{31a}$$

It is often convenient to use the notation

$$\nu(Q,x,\Omega)=a(Q,x,\Omega)/Q$$
$$=\frac{2}{\pi}\int_0^\infty dq\frac{\cos(qx)}{|\mathbf{q}|^2\epsilon(\mathbf{q},\Omega)}\ . \tag{31b}$$

Equations (28)–(31) are in agreement with earlier results[2] for $l\to\infty$. In the high-frequency–low-wave-number approximation, describing local, long-wavelength plasma behavior, we have $\epsilon(\mathbf{q},\Omega)\to\epsilon(\mathbf{0},\Omega)\to\epsilon(\Omega)$.

III. MAGNETIC-FIELD EFFECTS ON SHIELDING AND IMAGE PHENOMENA NEAR A SURFACE

Our treatment of static shielding phenomena will be focused on the role of quantum magnetic-field effects with a single bounding surface for a thick slab. In this, we will analyze the shielding integral

$$V(\mathbf{r},\,t\to\infty)$$
$$=(2\pi)^{-2}\int dx'\int d^2Q e^{i\bar{Q}\cdot\bar{R}}$$
$$\times K_Q(x,x';\Omega\to i0^+)U(\bar{\mathbf{Q}},x')\ , \tag{32}$$

where $U(\bar{\mathbf{Q}},x')$ is the two-dimensional (2D) Fourier transform of an impressed Coulombic impurity potential of strength Ze centered at $\mathbf{r}_0=(x_0,0,0)$. Our examination will treat contributions from the vicinity of an anisotropic Thomas-Fermi shielding pole $\sim Q_{\rm TF}$ at low wave numbers, and a Friedel-Kohn oscillatory branch-cut contribution at $2Q_F$ (Q_F is the Fermi wave number), which we take to be in a much higher wave-number regime $2Q_F\gg Q_{\rm TF}$, so that the singularities contribute with negligible interference. It is well known that at zero magnetic field the Friedel-Kohn oscillatory contribution is important at large distances from the impurity. Qualitatively, one may surmise this by expanding the shielded potential integrand in the vicinity of $2Q_F$ in powers of the small polarizability contribution $|q-2Q_F|\ln|q-2Q_F|$, whose long-range oscillatory contribution in position space is never quenched. The introduction of a strong magnetic field, however, leads to a qualitative change: In the anisotropic quantum strong field limit (all electrons in the lowest Landau level), $\hbar\omega_c>\zeta$ the branch-cut polarizability contribution $\sim\ln(q-2Q_F)$ is very large near $2Q_F$ (Appendix), precluding any possible expansion in powers of it, and in fact its largeness in the shielding integrand denominator diminishes the contribution from $\sim 2Q_F$, reducing the Friedel oscillatory shielding component in high magnetic field.

For a thick slab of solid-state plasma, with Coulombic source and field points at distances $x_0,x>(1/2Q_F)$ from the surface, we employ the semi-infinite "diagonal" approximation for $K_Q(x,x')$ given by Eq. (28) (zero frequency limit, $\Omega\to 0$) for the evaluation of $V(\mathbf{r},t\to\infty)$ in Eq. (32) to examine the effects of shielding on image phenomena. Executing the x' integrals involved we obtain a result[4] having four distinct analytic structures depending on whether the field point x and source point x_0 are within or outside of the plasma slab, as follows (J_0 is the Bessel function and $\Omega\to 0$ throughout for the static limit; also, recall $\nu=a/Q$):

Case I, $x<0$ and $x_0<0$:

$$V_{\rm I}=\frac{Ze}{|\mathbf{r}-\mathbf{r}_0|}+Ze\int_0^\infty dQ\,J_0(QR)\frac{Q\nu(Q,0)-1}{Q\nu(Q,0)+1}e^{-Q|x+x_0|}\ . \tag{33a}$$

Case II, $x>0$ and $x_0>0$:

$$V_{\rm II}=Ze\int_0^\infty dQ\,J_0(QR)Q\left[\nu(Q,x-x_0)+\nu(Q,x+x_0)\right.$$
$$\left.-\frac{2Q\nu(Q,x)\nu(Q,x_0)}{Q\nu(Q,0)+1}\right]. \tag{33b}$$

Case III, $x<0$ and $x_0>0$:

$$V_{\rm III}=2Ze\int_0^\infty dQ\,J_0(QR)\frac{Q\nu(Q,x_0)}{Q\nu(Q,0)+1}e^{-Q|x|}\ . \tag{33c}$$

Case IV, $x>0$, and $x_0<0$:

$$V_{\rm IV}=2Ze\int_0^\infty dQ\,J_0(QR)\frac{Q\nu(Q,x)}{Q\nu(Q,0)+1}e^{-Q|x_0|}\ . \tag{33d}$$

The bulk static dielectric function involved has been thoroughly examined,[5-7] and for the quantum strong-field limit ($\hbar\omega_c>\zeta$) it takes the zero-temperature form [Ref. 5(b)]

$$\epsilon(Q,q)=\epsilon_0-[4\pi e^2/(Q^2+q^2)](\rho/\hbar)(m/2q^2\zeta)^{1/2}\times e^{(\hbar Q^2/2m\omega_c)}\ln|(q-2Q_F)/(q+2Q_F)|\ , \tag{34}$$

where we have neglected higher-order terms $O(\hbar Q^2/2m\omega_c)^n$ with $n\geq 1$ for the examination of shielding at large transverse distances $\bar{R}$. Also, $\zeta=\hbar^2Q_F^2/2m$ is the Fermi energy, m is the effective mass, $\rho=m^{3/2}\omega_c\zeta^{1/2}/2^{1/2}\pi^2\hbar^2$ is the uncorrelated density expression for $\hbar\omega_c>\zeta$, ϵ_0 is the background dielectric constant, and ω_c is the cyclotron frequency. The quantity $a(Q,x)=a(Q,x,\Omega=0)$ is of central importance in the application of Eq. (28), and

$$a(Q,x)\equiv Q\nu(Q,x)=(Q/\pi)\int_{-\infty}^{\infty}dq\,e^{iqx}/[(q^2+Q^2)\epsilon(\mathbf{q})]\ , \tag{35}$$

due to the even property of $\epsilon(\mathbf{q})$. The analysis of the q integral of Eq. (35) is facilitated by noting that there are two types of singularities of the integrand, an anisotropic Thomas-Fermi shielding pole around $Q_{\rm TF}$ and branch points at $\pm 2Q_F$, which are well separated for $2Q_F\gg Q_{\rm TF}$. With this in view, we deform the q contour off the real axis as indicated in Fig. 2, to a large semicircle in the upper half q plane, thus encircling the isolated pole about $Q_{\rm TF}$ and encircling the vertical branch cuts originating at the branch points $\pm 2Q_F$ as shown. This yields two distinct contributions (recognizing that the semicircular parts of the contour produce null contributions): $a(Q,x)=a_{\rm TF}(Q,x)+a_{\rm FK}(Q,x)$. The Thomas-Fermi pole contribution is

$$a_{\rm TF}(Q,x)=(Q/\pi)\oint_{(\rm TF\ pole)}dq\,e^{iqx}/[(q^2+Q^2)\epsilon(\mathbf{q})] \tag{36}$$

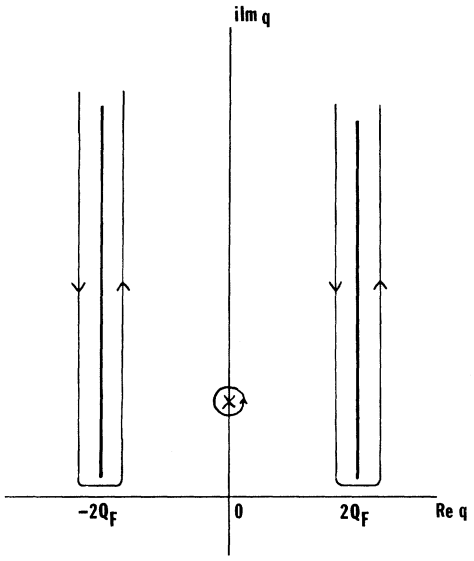

FIG. 2. Contour for the q integration of Eq. (35).

and in this low-wave-number regime $q\sim Q_{\rm TF}\ll 2Q_F$ we may approximate Eq. (34) using an expansion in powers of wave number as[6,7]

$$\epsilon(\mathbf{q})=\epsilon_0\{1-[4\pi e^2/\epsilon_0(q^2+Q^2)]\times(-\partial\rho/\partial\zeta+Aq^2+BQ^2)\}\ , \tag{37}$$

where an anisotropic effective Thomas-Fermi shielding length is manifested by the nonidentical expansion parameters A,B: We employ the notation $Q_{\rm TF}^2=4\pi e^2\partial\rho/\partial\zeta$ and A,B are given in terms of the bulk electron density ρ and bulk energy density σ by[6,7]

$$A=(\hbar^2/12m)\partial^2\rho/\partial\zeta^2\ , \tag{38a}$$

$$B=[1/m\omega_c^2][\partial\sigma/\partial\zeta-\rho]\rightarrow[1/m\omega_c^2][(\hbar\omega_c/2)\partial\rho/\partial\zeta-\rho]\ . \tag{38b}$$

The last part of Eq. (38b) pertains to the quantum strong-field limit with $\sigma\rightarrow\hbar\omega_c\rho/2$. Corresponding results for A,B,ρ,σ, etc. for arbitrary magnetic field strength and temperature are given in Refs. 6 and 7. The q integration of $a_{\rm TF}(Q,x)$ involves only a simple pole, with the result:

$$a_{\rm TF}(Q,x)=[Q/(C^2+E_0^2Q^2)^{1/2}]\exp\{-|z|[(C^2+E_0^2Q^2)^{1/2}/(1-4\pi e^2A/\epsilon_0)^{1/2}\epsilon_0]\}\ , \tag{39}$$

where

$$C^2=\epsilon_0(1-4\pi e^2A/\epsilon_0)Q_{\rm TF}^2 \tag{40}$$

and

$$E_0^2=\epsilon_0^2(1-4\pi e^2A/\epsilon_0)(1-4\pi e^2B/\epsilon_0)\ . \tag{41}$$

Qualitatively, we note that $C\sim\epsilon_0^{1/2}Q_{\rm TF}$, $E_0\sim\epsilon_0$, and for $Q<Q_{\rm TF}$ we have

$$a_{\rm TF}(Q,x)\sim(Q/\epsilon_0^{1/2}Q_{\rm TF})e^{-|x|Q_{\rm TF}/\epsilon_0^{1/2}} \quad \text{with } a_{\rm TF}(Q,0)\sim(Q/\epsilon_0^{1/2}Q_{\rm TF}) .$$

There are two identical branch-cut contributions to $a_{\rm FK}(Q,x)$ from the contour segments in the vicinity of $\pm 2Q_F$, which may be obtained by setting $q=(2Q_F+iu)$, and writing

$$a_{\rm FK}(Q,x)=(2Q/\pi){\rm Re}e^{2iQ_Fx}\oint_{(2Q_F\ \text{branch})}du\ e^{-ux}/[(2Q_F+iu)^2+Q^2]\epsilon(\mathbf{q}) . \tag{42}$$

Introducing $\epsilon(\mathbf{q})=\epsilon(Q,\,2Q_F+iu)$ of Eq. (34) to explicitly exhibit the role of $\ln(q-2Q_F)\to\ln u$, and taking account of its discontinuity across the vertical branch cut of Fig. 2, the integrals on the two sides of the cut combine to yield

$$a_{\rm FK}(Q,x)=-\frac{2Q}{\epsilon_0}b\ {\rm Re}\left[e^{2iQ_Fx}\int_0^\infty du\frac{(2Q_F+iu)e^{-ux}}{\left[(2Q_F+iu)^3+Q^2(2Q_F+iu)+b\ln\left[\frac{4Q_F+iu}{u}\right]\right]^2+\left[\frac{\pi b}{2}\right]^2}\right] , \tag{43}$$

where

$$b\equiv\frac{4\pi e^2\rho}{\hbar\epsilon_0}\left[\frac{m}{2\zeta}\right]^{1/2}\exp(-\hbar Q^2/2m\omega_c)\equiv b_0\exp(-\hbar Q^2/2m\omega_c) .$$

The asymptotic behavior for large $x\gg 1/2Q_F$ is dominated by behavior near the u origin where $\ln u$ is large in the denominator of the integrand, whence (set $u'=u/4Q_F$)

$$a_{\rm FK}(Q,x)\approx-\frac{Q}{\epsilon_0}b\ {\rm Re}\left[e^{2iQ_Fx}\int_0^\infty du'\frac{e^{-4Q_Fu'x}}{[(2Q_F)^3+Q^2(2Q_F)-b\ln u']^2+\left[\frac{\pi b}{2}\right]^2}\right] \tag{44}$$

and we obtain the result

$$a_{\rm FK}(Q,x)\approx-\frac{Q}{b\epsilon_0}\cos(2Q_Fx)\int_0^\infty du'\frac{e^{-4Q_Fxu'}}{(\ln u')^2} . \tag{45a}$$

Further information concerning the evaluation of this integral for $4Q_Fx\gg 1$ is presented in the Appendix, where we show that

$$a_{\rm FK}(Q,x)\approx-\frac{Q}{b\epsilon_0}\frac{1}{4Q_Fx}\frac{\cos(2Q_Fx)}{[\ln(4Q_Fx)^2]}\times\left[1+O\left[\frac{1}{\ln(4Q_Fx)}\right]\right] . \tag{45b}$$

Above, we have also set $Q\to 0$ corresponding to large $\bar{R}$ in the sense that $R^2>\hbar/2m\omega_c\sim r_c^2$ (r_c is the radius of the lowest Landau state). In applying this to the determination of $a_{\rm FK}(Q,0)$ involving $x\to 0$, we bear in mind that the validity of the diagonal approximation is contingent upon $2Q_Fx>1$, so that quantum interference effects associated with wave-function reflection at the boundary may be neglected. Therefore Eq. (45) may be understood consistently as making a vanishingly small contribution to $a_{\rm FK}(Q,0)$ in the limit of small x (modulo $x>1/2Q_F$) within the framework of the diagonal approximation. A more careful examination of $a_{\rm FK}(Q,0)$ starting from Eq. (42), eliminating the restriction $x>1/2Q_F$ in the limit $x\to 0$, reveals a featureless and small contribution to $a_{\rm FK}(Q,0)$ lacking Friedel-Kohn oscillatory structure, which may be safely ignored as indicated above. Nevertheless, a fully proper treatment should restore the nondiagonal quantum interference terms which have been eliminated in this diagonal analysis. Finally, we note that in the absence of a significant branch cut contribution

$$a(Q,0)=a_{\rm TF}(Q,0) , \tag{46}$$

the Thomas-Fermi pole is the major contributor to $a(Q,0)$. It is important to note that to the extent that shielding phenomena are determined by the Thomas-Fermi (Debye) pole, there is no need to limit consideration to the quantum strong-field limit, and arbitrary lower magnetic-field strength regimes are admissible, including nondegeneracy as well as degeneracy, provided the results of Refs. 5–7 are employed. On the other hand, for large $x>1/2Q_F$, we combine $a_{\rm TF}(Q,x)+a_{\rm FK}(Q,x)$ to obtain the result for $a(Q,x)$ as

$$a(Q,x)=\frac{Q}{\epsilon_0}\frac{e^{-[Q^2+Q_{\rm TF}^2/\epsilon_0]^{1/2}x}}{[Q^2+Q_{\rm TF}^2/\epsilon_0]^{1/2}}-\frac{Q}{b_0\epsilon_0}\frac{1}{4Q_Fx}\frac{\cos(2Q_Fx)}{[\ln(4Q_Fx)]^2} , \tag{47}$$

where $b_0\equiv b(Q=0)$.

It is straightforward to carry out the determination of the shielded potential $V(\mathbf{r})$ in Eq. (33) using the evaluation of $a(Q,x)$ discussed above. For case I, in which both the source and field points are outside the medium in vacuum ($x<0$, $x_0<0$), there is no charge present in the outside region to support a Friedel-Kohn wiggle (i.e., spatial oscillatory structure) of density or potential, which thus cannot occur. Mathematically, this is mani-

fested in the fact that only $a(Q,0)$ appears in $V_{\rm I}(\mathbf{r})$ as given by Eq. (33a), and $a(Q,0)=a_{\rm TF}(Q,0)$ [Eq. (46)] and hence $V_{\rm I}(\mathbf{r})$ is therefore determined by the Thomas-Fermi pole alone and is devoid of Friedel-Kohn oscillatory phenomena. The Q integral of Eq. (33a) may be evaluated using Eq. (39) [$a_{\rm TF}(Q,0)=Q(C^2+E_0^2Q^2)^{-1/2}$], taking the form

$$V_{\rm I}(\mathbf{r})=Ze\int_0^\infty dQ\,J_0(QR)(e^{-Q|x-x_0|}-e^{-Q|x+x_0|}) + \frac{2Ze}{C}\int_0^\infty dQ\,QJ_0(QR)e^{-Q|x+x_0|} \times\left[\frac{(1+Q^2E_0^2/C^2)^{1/2}-Q/C}{1-Q^2(1-E_0^2)/C^2}\right]. \tag{48}$$

The first integral is well known (Ref. 8, p. 712, No. 6.623.1), and it describes the bare source potential and its ideal image. Evaluating the last integral of Eq. (48) for large separations between the impurity, image, and field points, $Q_{\rm TF}|x\pm x_0|\gg 1$, $Q_{\rm TF}R\gg 1$, we expand the term in large parentheses in powers $Q\ll Q_{\rm TF}\ll 2Q_F$, and retaining only the leading term we find

$$V_{\rm I}(\mathbf{r})=\frac{Ze}{(R^2+|x-x_0|^2)^{1/2}}-\frac{Ze}{(R^2+|x+x_0|^2)^{1/2}} +\frac{2Ze}{C}\frac{|x+x_0|}{(R^2+|x+x_0|^2)^{3/2}}. \tag{49}$$

We note that as a result of nonlocal static shielding effects, the coefficient of the second (ideal image) term in Eq. (49) is -1 and *not* the conventional image strength factor $(1-\epsilon_0)/(1+\epsilon_0)$. One could anticipate this result directly from Eq. (33a) by noting the smallness of $a(Q,0)\sim a_{\rm TF}(Q,0)\sim(Q/\epsilon_0^{1/2}Q_{\rm TF})\ll 1$ for large separations. However, dependence on the background dielectric constant ϵ_0 is carried in the third term in the structure of C and E_0, and the same may be said for the quantum magnetic field parameter $\hbar\omega_c$. Of course, semiclassical and classical magnetic field parameters will not enter Thomas-Fermi (Debye) static shielding phenomena at any (arbitrary) magnetic field strength since the Lorentz force of classical dynamics cannot do work and it is therefore incapable of supplying energy which would be required for a redistribution of static shielding charge.

We may examine $V_{\rm I}(\mathbf{r})$, Eq. (48), for separations that are small in the sense that $Q_{\rm TF}|x\pm x_0|<1$, $Q_{\rm TF}R\ll 1$ [notwithstanding our commitment to $2Q_F(x,x_0)\gg 1$ and $R>r_c$] by expanding the last integrand factor of Eq. (48) in parentheses in inverse powers of Q ($Q_{\rm TF}<Q<2Q_F$), obtaining $[\ ]\to[C/Q(1+E_0)]$, with the integrated result

$$V_{\rm I}(\mathbf{r})=\frac{Ze}{(R^2+|x-x_0|^2)^{1/2}} +\left[\frac{1-E_0}{1+E_0}\right]\frac{Ze}{(R^2+|x+x_0|^2)^{1/2}}. \tag{50}$$

The image strength factor here, $(1-E_0)/(1+E_0)$, is only slightly modified from what it would be in the absence of static shielding of the image. This is physically reasonable because the image distance behind the surface is too short to accommodate an assemblage of shielding charges, and shielding is thus rendered ineffective.

It is of interest to treat the case $R\to 0$ (modulo $R>r_c\sim 0$) in which $J_0(QR)\to 1$ in Eq. (48) for arbitrary values of $|x\pm x_0|$, which bridges the large and small separation regimes discussed above. This case is analytically tractable in closed form for $E_0=1$ (neglect quantum effects and $\epsilon_0\to 1$; $C\sim Q_{\rm TF}$) with the result

$$V_{\rm I}(\mathbf{r})=\frac{Ze}{|x-x_0|}-\frac{Ze}{|x+x_0|}-\frac{4Ze}{C^2|x+x_0|^3} +I(R=0), \tag{51}$$

where

$$I(R=0)\equiv\frac{2Ze}{C^2}\int_0^\infty dQ\,Qe^{-Q|x+x_0|}(Q^2+C^2)^{1/2} =\frac{2Ze}{C^2}\left[C^2+\frac{\partial^2}{\partial\mu^2}\right] \times\left[\frac{\pi C}{2}[\mathrm{H}_1(C\mu)-\mathrm{N}_1(C\mu)]-C\right] \tag{52}$$

evaluated at $\mu\equiv|z+z_0|$. In this, H_1 is a Struve function and N_1 is a Neumann function (Ref. 8, p. 316, No. 3.366.3).

$V_{\rm I}(\mathbf{r})$, having $x<0$ and $x_0<0$ is determined by the Thomas-Fermi (Debye) pole and is devoid of Friedel-Kohn wiggle behavior. As pointed out above, in such cases the results we have obtained describe all regimes of magnetic-field strength (not just the quantum strong-field limit) provided that the identifications of Refs. 5–7 are employed for lower fields and nondegenerate as well as degenerate statistics.

Focusing attention on the "cross-boundary" shielding cases where either source point $x_0>0$ is inside the medium while field point $x<0$ is outside (case III) or, on the other hand, where field point $x>0$ is inside the medium while source point $x_0<0$ is outside (case IV), we note that the inside point in either case involves perturbed electron density which is capable of supporting a Friedel-Kohn wiggle of the potential as a function of the inside point. Noting that such a Friedel-Kohn wiggle dominates the large-separation behavior of $a(Q,x)\sim a_{\rm FK}(Q,x)<1$, and further recalling that $a(Q,0)\sim a_{\rm TF}(Q,0)\ll 1$, we may approximate $V_{\rm III}(\mathbf{r})$ for case III [Eq. (33c)] as

$$V_{\rm III}(\mathbf{r})\cong 2Ze\int_0^\infty dQ\,J_0(QR)a(Q,x_0)e^{-Q|x|} \tag{53a}$$

and considering large R separation as well as large x,x_0, we have [recall from Eq. (35) the definition $\nu(Q,x)=a(Q,x)/Q$; $\nu_{\rm FK}(Q,x)=a_{\rm FK}(Q,x)/Q$]

$$V_{\rm III}(\mathbf{r})\cong 2Ze\nu_{\rm FK}(0,x_0)|x|/(R^2+x^2)^{3/2}. \tag{53b}$$

Similarly, we approximate $V_{\rm IV}(\mathbf{r})$ for case IV [Eq. (33d)] with large separation as

$$V_{\rm IV}(\mathbf{r})\cong 2Ze\nu_{\rm FK}(0,x)|x_0|/(R^2+x_0^2)^{3/2}. \tag{54}$$

Friedel-Kohn wiggle behavior is manifested through $\nu_{FK}(0,x_0)$ and $\nu_{FK}(0,x)$ as functions of source point x_0 and field point x in $V_{III}(\mathbf{r})$ and $V_{IV}(\mathbf{r})$, respectively.

Finally, we consider $V_{II}(\mathbf{r})$ for case II in which both the source point $x_0>0$ and field point $x>0$ are inside the medium. Qualitaively, we may expect Friedel-Kohn wiggle behavior of the potential in its dependence on both source and field points, since both points are inside where the perturbed density is capable of sustaining such phenomena. For large separations, $a(Q,x \text{ or } x_0) \sim a_{FK}(Q,x \text{ or } x_0)<1$, and again $a(Q,0)\sim a_{TF}(Q,0)\ll 1$, so that $V_{II}(\mathbf{r})$ [Eq. (33b)] may be approximated as

$$V_{II}(\mathbf{r})\approx Ze\int_0^\infty dQ\, J_0(QR)[a(Q,x-x_0)+a(Q,x+x_0) -2a(Q,x)a(Q,x_0)]\ . \quad (55)$$

The first and second terms of the integrand of $V_{II}(\mathbf{r})$ in Eq. (55), which are exact, correspond to the bulk shielded potentials of an impurity charge sited at $(x_0,0,0)$ and of an image charge of identical strength sited at the image position $(-x_0,0,0)$, respectively. It is worthwhile noting that the approximation Eq. (45b) for $a_{FK}(Q,x)$ leads to Friedel oscillatory contributions which exhibit high Q-wave-number divergences in the first two terms of the form

$$Ze[\nu_{FK}(0,x-x_0)+\nu_{FK}(0,x+x_0)] \times\left[\int_0^\infty d\xi\,\xi J_0(\xi)\right]\Big/R^3$$

due to the low-wave-number approximations undertaken in deriving Eq. (45b). This limitation also results in a similar high Q-wave-number divergence in the third term of $V_{II}(\mathbf{r})$ in Eq. (55), which is of the form

$$-2Ze\nu_{FK}(0,x)\nu_{FK}(0,x_0)\left[\int_0^\infty d\xi\,\xi^2 J_0(\xi)\right]\Big/R^3\ .$$

The restoration of higher Q-wave-number dependence requisite for removal of the divergences in the branch-out integral (associated with Friedel-Kohn wiggle oscillatory shielding phenomena) involves due consideration of a Coulomb pole term $\sim[(2Q_F)^2+Q^2]$ heretofore neglected in the denominator of the integrand of $a_{FK}(Q,x)$ in Eqs. (43) and (44). While this substantially complicates analytical evaluation, we may gain an appreciation of its role from an earlier ordinary Hartree-Fock-type treatment of the Friedel wiggle in the quantum strong-field limit, which showed that the Coulomb pole couples the anisotropic branch cut to source-field displacements parallel to the surface such that for large displacements the Friedel wiggle contribution to the shielded potential dies off very rapidly with an exponential envelope factor $\exp(-2Q_FR)$.[5-7] Consequently, for such large parallel displacements in the first two bulk terms of $V_{II}(\mathbf{r})$ in Eq. (55), the more slowly decaying exponential falloff $\exp(-Q_{TF}R)$ of the bulk Thomas-Fermi (Debye) contribution dominates the statically shielded potential. Similarly one may expect the third term of $V_{II}(\mathbf{r})$ in Eq. (55) to yield a negligible Friedel wiggle shielding contribution for large $2Q_FR\gg 1$.

On the other hand, for displacements along the magnetic-field direction and perpendicular to the surface $R\to 0$, the exponential envelope factor $\exp(-2Q_FR)\to 1$ is unity, signaling the dominance of the highly anisotropic Friedel wiggle contribution to the shielded potential over the Thomas-Fermi (Debye) contribution. An ordinary Hartree-Fock calculation[9] of this Friedel wiggle in the presence of a surface was presented in Ref. 9, including the role of quantum interference effects, and also in Ref. 10 a numerical RPA calculation is given for the Friedel wiggle shielded potential in the presence of a sur-

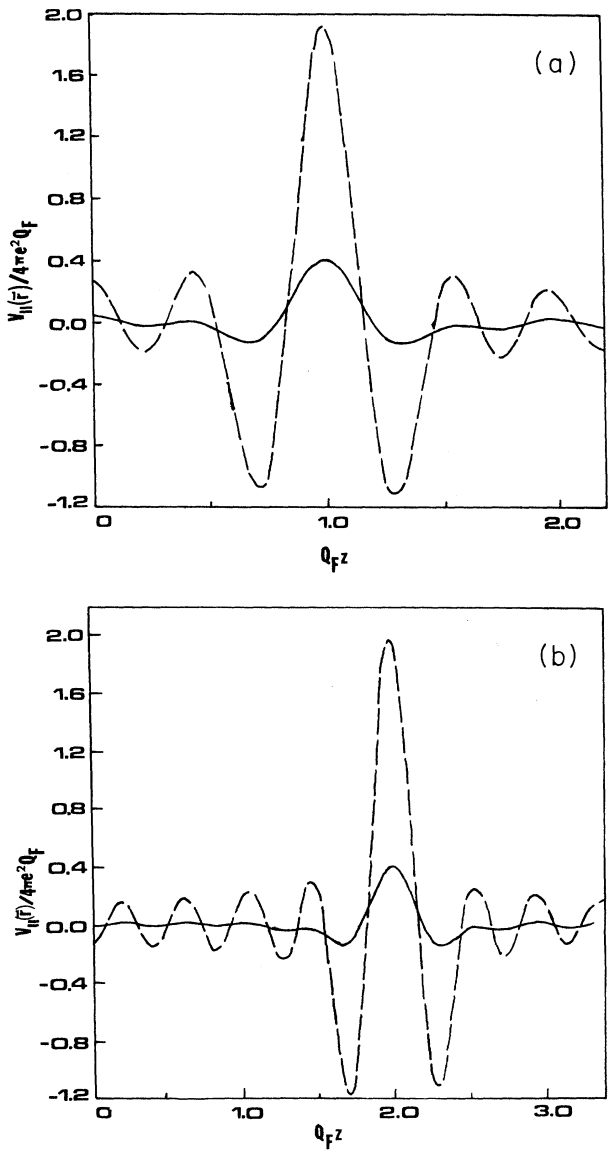

FIG. 3. Plots of the "inside" shielded potential $V_{II}(R=0,x)/(4\pi e^2Q_F)$ as a function of (Q_Fx) for a Coulombic impurity sited within the plasma on the axis at a distance (a) $x_0=Q_F^{-1}$ and (b) $x_0=2Q_F^{-1}$ from the surface. The solid curve is for a background dielectric constant $\epsilon_0=10.94$ and the dashed curve is for $\epsilon_0=1$. The magnetic field is $H=10^5$ G.

face, but without quantum interference effects.[10] Here, we present a similar numerical RPA evaluation of the full "inside" shielded potential embodying the Freidel wiggle contribution along with the Thomas-Fermi (Debye) contribution based on Eq. (33b) for $R=0$, again without quantum interference effects, but including the role of the background dielectric constant appropriate to semiconductors in which the quantum strong-field limit can be achieved.

The appropriate bulk dielectric function $\epsilon(Q,q)$ for such a full static shielding analysis involves more structure than is given in Eq. (34), even for the strong-field limit, since the higher-order terms $O(\hbar Q^2/2m\omega_c)^n$ cannot be neglected out-of-hand with $R\rightarrow 0$, and the appropriate form for $\epsilon(Q,q)$ is given in Ref. 5(b). The numerical results for $V_{\rm II}(\mathbf{r})$ are shown in Figs. 3a and 3(b) for $R=0$ and values of $Q_F x_0 \gtrsim 1$, so that the role of omitted quantum interference terms may be expected to be relatively unimportant in accordance with the results of Ref. 9. In the calculations, we take the magnetic field to be $H=10^5$ G, and for GaAs we use an electron effective mass $m=0.0665m_e$, bulk density $\rho=10^{16}$ cm^{-3}, $\epsilon_0=10.94$, Fermi wave number $Q_F=0.0013$ Å^{-1}, chemical potential $\zeta=9.65\times10^{-5}$ eV, and cyclotron frequency $\omega_c=2.65\times10^{13}$ sec^{-1}. For these values $\hbar\omega_c>\zeta$ and the quantum strong-field limit is achieved with only the lowest Landau state occupied. The Friedel-Kohn wiggle is prominent in the RPA shielded potential shown as a function of x distance from the boundary for $R=0$ in all parts of Fig. 1 for various values of $Q_F x>1$. In addition to the solid curves which show $V_{\rm II}(x)$ for GaAs with $\epsilon_0=10.94$, the corresponding results for $\epsilon_0\rightarrow 1$ (but with all other numbers characteristic of GaAs the same as indicated above) are shown in dashed curves to emphasize the importance of incorporating the proper value of the background dielectric constant ϵ_0.

IV. SUMMARY

We have analyzed the electrostatic fields and dielectric response of a finite slab of Landau quantized magnetoplasma subject to the boundary condition of specular reflection at the slab faces (infinite barrier model). In this, the RPA inverse dielectric function has been constructed quite generally, avoiding any commitment to potentials having special symmetry across the slab, and the role of "nondiagonal" quantum interference effects has been included. Special limits and approximations of particular interest for $K(1,2)$ are explicitly determined.[11] This rather formal work will find many useful applications for a finite slab, including the analysis of fast particle energy loss to a film to be presented in a companion paper,[3] and a variety of other surface response properties governed by the longitudinal dielectric response function of the slab.

Our analysis of magnetic-field effects on static shielding phenomena and images in the vicinity of a magnetoplasma surface has been exhaustive. In this, we have treated all cases and phenomena of interest in a magnetic field, including shielded image potentials when both source and field points are outside the plasma surface, and "cross-boundary" shielding when one of the points is inside the plasma boundary and the other is outside. Finally, we studied the surface-corrected bulk shielding when both the source and field points are inside the plasma surface, presenting a numerical study for a realistic sample. Our shielding work in all cases incorporates the role of Thomas-Fermi (Debye) shielding phenomena and Friedel-Kohn wiggle shielding effects for a highly anisotropic bounded magnetoplasma in the quantum strong-field limit. This case, in which only the lowest Landau eigenstate is occupied, is more complicated than its zero-field isotropic counterpart because the quantum strong-field limit polarizability becomes large at $q\sim 2Q_F$, rather than small. Notwithstanding this, we have obtained both closed form analytical results, as well as numerical results, for the anisotropic Friedel-Kohn wiggle shielding contribution in the vicinity of a surface, as presented in Sec. III.

Beyond the formal considerations, some interesting shielding phenomenology in the presence of a bounding surface and a magnetic field has been elucidated in our analysis. For the "outside" case, $V_{\rm I}(\mathbf{r})$ exhibits image potential structure whose strength is substantially changed from the conventional (local) image strength factor $(1-\epsilon_0)/(1+\epsilon_0)$ to image strength (-1) for large distances $2Q_F>Q_{\rm TF}>(R^{-1},|z\pm z_0|^{-1})$ due to nonlocal static shielding. On the other hand, for distances too small $(Q_{\rm TF}|z\pm z_0|<1,\ Q_{\rm TF}R\ll 1)$ to accommodate an assemblage of shielding charges, the conventional local image strength factor again emerges, because the shielding is thus rendered ineffective. Our exact treatment of the special case $R=0$ bridges the large-and small-distance regimes for $|z\pm z_0|$ discussed separately above. In these considerations, an anisotropic Thomas-Fermi pole (modified by quantum magnetic-field effects) dominates shielding phenomena since the absence of charge density outside the boundary precludes any possibility of supporting a Friedel-Kohn wiggle shielding contribution.

In the "cross-boundary" shielding cases where either the source point or the field point is inside the medium (and the other point is outside), the inside point in either case involves perturbed electron density. This provides the capability of supporting a Friedel-Kohn wiggle contribution (as a function of the inside point), which dominates the long-distance shielded potential $V_{\rm III}, V_{\rm IV}$ across the boundary. Our explicit analytic evaluation of the Friedel-Kohn wiggle shielding integral shows that the highly anisotropic quantum strong-field limit involves a polarizability whose largeness in the shielding integrand denominator at $q\sim 2Q_F$ diminishes the high field FK wiggle.

For the "inside" shielded potential $V_{\rm II}$, with both field and source points inside the medium, the charge density perturbation of the medium again sustains a Friedel wiggle component of the shielded potential. Under the high magnetic-field conditions of this quantum strong-field limit study, the "inside" Friedel wiggle dies off exponentially for $R>1/(2Q_F)$ due to a Coulomb pole which couples the anisotropic branch cut to source-field displacements parallel to the surface, leading to an envelope fac-

tor $\exp(-2Q_F R)$, and then the more slowly decaying Debye-Thomas-Fermi exponential falloff $\exp(-Q_{TF}R)$ characterizes shielding. However, for $R<1/(2Q_F)$ the Friedel wiggle is in fact dominant over the Thomas-Fermi contribution, and the shielded potential for $R=0$ is evaluated numerically here including the role of the background dielectric constant ϵ_0. The results presented in Fig. 3 for $R=0$ exhibit the prominence of Friedel oscillations, and they also emphasize the importance of incorporating the proper value of ϵ_0 for semiconductors.

ACKNOWLEDGMENTS

This work was supported in part by the Natural Sciences and Engineering Research Council of Canada and by the University of Lethbridge Research Fund (G.G.) The authors thank Dr. M. L. Glasser for helpful discussions.

APPENDIX

We provide further detail about the evaluation of the integral of Eq. (45). Setting $\lambda=4Q_F x$, it is of the form ($\alpha=0,\beta=2$)

$$I=\int_0^\infty du'\,(u')^\alpha e^{-\lambda u'}/(-\ln u')^\beta$$
$$=(1/\lambda^{\alpha+1})\int_0^\infty dt\,t^\alpha e^{-t}/(\ln\lambda-\ln t)^\beta \quad \text{(A1)}$$

where we have set $u'=t\lambda^{-1}$. Alternatively written,

$$I=(1/\lambda^{\alpha+1})[1/(\ln\lambda)^\beta]$$
$$\times\int_0^\infty dt\,t^\alpha e^{-t}(1-\ln t/\ln\lambda)^{-\beta}\,, \quad \text{(A2)}$$

an expansion in inverse powers of $\ln\lambda\gg1$ (for $4Q_F x\gg1$) yields

$$I\cong[\Gamma(\alpha+1)/\lambda^{\alpha+1}][1/(\ln\lambda)^\beta$$
$$+\beta g(\alpha+1)/(\ln\lambda)^{\beta+1}\cdots]\,, \quad \text{(A3)}$$

where

$$g(\alpha+1)=[1/\Gamma(\alpha+1)]\int_0^\infty dt\,e^{-t}t^\alpha\ln t$$
$$=[1/\Gamma(\alpha+1)]\left[(d/dz)\int_0^\infty dt\,e^{-t}t^{-1}(e^{z\ln t})\right]_{z=\alpha+1}$$
$$=[1/\Gamma(\alpha+1)]\left[(d/dz)\int_0^\infty dt\,e^{-t}t^{z-1}\right]_{z=\alpha+1}=\Gamma'(\alpha+1)/\Gamma(\alpha+1)=\psi(\alpha+1)\,. \quad \text{(A4)}$$

Here, $\Gamma(x)$ is the gamma function and $\psi(x)$ is the digamma function.[8] This provides us with the leading term of the evaluation I [Eq. (45)] and its next correction as

$$I\cong[\Gamma(\alpha+1)/\lambda^{\alpha+1}][1/(\ln\lambda)^\beta+\beta\psi(\alpha+1)/(\ln\lambda)^{\beta+1}+\cdots] \quad \text{(A5)}$$

for $\lambda=4Q_F x\gg1$. It should be noted that in our case, $\alpha=0$ and $\beta=2$, and the requisite value of the digamma function in the correction is $\psi(1)=-C$ where C is Euler's constant.[8]

[1]D. M. Newns, Phys. Rev. B **1**, 3304 (1970).

[2](a) The inverse dielectric function for a *semi-infinite* quantum plasma was treated in N. J. M. Horing, E. Kamen, and H. L. Cui, Phys. Rev. B **32**, 2184 (1985). (b) In the diagonal approximation (no quantum interference effects) the inverse dielectric function for a *finite slab* was determined by F. Bechstedt and R. Enderlein, Phys. Status Solidi B **131**, 53 (1985). Also, see Ref. 4.

[3]G. Gumbs and N. J. M. Horing, following paper, Phys. Rev. B **43**, 2119 (1991).

[4]F. Bechstedt, R. Enderlein, and D. Reichardt, Phys. Status Solidi B **117**, 261 (1983).

[5](a) N. J. Horing, Ann. Phys. (N.Y.) **31**, 1 (1965); (b) N. J. Horing, Phys. Rev. **186**, 434 (1969), Appendix.

[6]N. J. Horing, Ann. Phys. (N.Y.) **54**, 405 (1969).

[7]N. J. Horing, J. Phys. Soc. Jpn. Suppl. **21**, 704 (1966).

[8]I. S. Gradshteyn and I. M. Ryzhik, *Tale of Integrals, Series and Products* (Academic, New York, 1965).

[9]G. Gumbs, Phys. Rev. B **27**, 7136 (1983).

[10]G. Gumbs and D. J. W. Geldart, Phys. Rev. B **29**, 5445 (1984).

[11]In connection with the application of our finite-thickness slab results to static shielding in the semi-infinite single-surface limit, it is appropriate to refer the interested reader to other important works directed at this limit, albeit in the absence of a magnetic field. J. W. Gadzuk, J. Phys. Chem. Solids **30**, 2307 (1969); D. E. Beck, V. Celli, G. LoVecchio, and A. Magnaterra, Nuovo Cimento B **LXVIII** (2), 230 (1970); D. E. Beck and V. Celli, Phys. Rev. B **2**, 2955 (1970); J. Heinrichs, *ibid.* B **8**, 1346 (1973); S. Peter Apell and David R. Penn, *ibid.* **34**, 6612 (1986).